



HAL
open science

Glenohumeral contact force during flat and topspin tennis forehand drives

Yoann Blache, Thomas Creveaux, Raphaël Dumas, Laurence Cheze, Isabelle Rogowski

► **To cite this version:**

Yoann Blache, Thomas Creveaux, Raphaël Dumas, Laurence Cheze, Isabelle Rogowski. Glenohumeral contact force during flat and topspin tennis forehand drives. *Sports Biomechanics*, 2017, 16 (1), pp.127 - 142. 10.1080/14763141.2016.1216585 . hal-01926636

HAL Id: hal-01926636

<https://univ-lyon1.hal.science/hal-01926636>

Submitted on 19 Nov 2018

HAL is a multi-disciplinary open access archive for the deposit and dissemination of scientific research documents, whether they are published or not. The documents may come from teaching and research institutions in France or abroad, or from public or private research centers.

L'archive ouverte pluridisciplinaire **HAL**, est destinée au dépôt et à la diffusion de documents scientifiques de niveau recherche, publiés ou non, émanant des établissements d'enseignement et de recherche français ou étrangers, des laboratoires publics ou privés.

1 **Glenohumeral contact force during flat and topspin tennis forehand drives**

2 Yoann Blache¹, Thomas Creveaux¹, Raphaël Dumas², Laurence Chèze², Isabelle Rogowski¹

3

4 ¹ Inter-University Laboratory of Human Movement Biology, University of Lyon, Lyon,
5 France

6

7 ² Biomechanics and Impact Mechanics Laboratory, University of Lyon, Lyon, France

8

9 Corresponding author: Yoann Blache, yoann.blache@univ-lyon1.fr

10

11

12 **Abstract**

13 The primary role of the shoulder joint in tennis forehand drive is at the expense of the
14 loadings undergone by this joint. Nevertheless, few studies investigated glenohumeral (GH)
15 contact forces during forehand drives. The aim of this study was to investigate GH
16 compressive and shearing forces during the flat and topspin forehand drives in advanced
17 tennis players. 3D kinematics of flat and topspin forehand drives of 11 advanced tennis
18 players were recorded. The Delft Shoulder and Elbow musculoskeletal model was
19 implemented to assess the magnitude and orientation of GH contact forces during the
20 forehand drives. The results showed no differences in magnitude and orientation of GH
21 contact forces between the flat and topspin forehand drives. The estimated maximal GH
22 contact force during the forward swing phase was 3573 ± 1383 N, which was on average 1.25
23 time greater than during the follow-through phase, and 5.8 times greater than during the
24 backswing phase. Regardless the phase of the forehand drive, GH contact forces pointed
25 toward the anterior-superior part of the glenoid therefore standing for shearing forces.
26 Knowledge of GH contact forces during real sport tasks performed at high velocity may
27 improve the understanding of various sport-specific adaptations and causative factors for
28 shoulder problems.

29

30 **Keywords:** Glenohumeral contact force; shoulder; musculoskeletal model; racket sports;
31 anterior-superior glenoid shearing force

32

33 **Introduction**

34 Playing tennis applies repeated high loads onto the upper limb joints, especially onto the
35 shoulder complex (Elliott, Fleisig, Nicholls, & Escamilia, 2003). If the serve places the tennis
36 player at the highest risk for impingements at the shoulder (Charbonnier, Chague, Kolo, &
37 Ladermann, 2015), repeated powerful forehand drives may also be a cause of shoulder
38 problems.

39 The achievement of a forehand drive requires three successive phases: a slow backswing to
40 place the body at an optimal pose before the drive, a rapid forward swing to accelerate the
41 racket head for impact, and a follow-through to slowdown the upper limb-racket complex
42 (Ryu, McCormick, Jobe, Moynes, & Antonelli, 1988). Two techniques of forehand drives are
43 mainly used by advanced tennis players: the flat and topspin. The main difference between the
44 two techniques is the racket path during the forward swing. For the flat forehand drive, the
45 racket is mainly moved horizontally, while, for the topspin shot, the racket is first moved
46 downward, then upward until ball impact. Such differences generate a higher vertical velocity
47 of the racket head at impact for topspin than for flat forehand drives (Takahashi, Elliott, &
48 Noffal, 1996). Nevertheless, whatever the technique used and according to the kinetic chain
49 concept described by Elliott and Marsh (1989), the racket head velocity at impact is a result of
50 the cumulative force production at successive body joints. In this context, shoulder motions
51 have a high contribution in the total force production. Takahashi et al. (1996) indeed observed
52 that the shoulder complex accounts for 60% of the upper limb contribution to the racket head
53 velocity during the forward swing phase. The role of the shoulder seems to remain similar

54 whatever the forehand drive technique, i.e. flat, topspin or lob (Takahashi et al., 1996), the
55 shot velocity (Seeley, Funk, Denning, Hager, & Hopkins, 2011), or the skill level (Landlinger,
56 Lindinger, Stoggl, Wagner, & Muller, 2010).

57 The primary contribution of the shoulder joint in the racket velocity generation is at the
58 expense of the loadings undergone by this joint. Indeed, the great shoulder joint amplitude
59 and velocity required during the forward swing and follow through phases, i.e. humeral
60 horizontal adduction and internal rotation (Marshall & Elliott, 2000), may lead to high
61 shoulder contact forces. To our knowledge, few studies investigated the loading undergone by
62 the shoulder during forehand drives. Two studies investigated the shoulder loadings by
63 computing the net joint moment/power at the humero-thoracic joint (Bahamonde & Knudson,
64 2003; Creveaux, Dumas, Cheze, Mace, & Rogowski, 2013a). Bahamonde and Knudson
65 (2003) observed that the horizontal adduction component was the greatest shoulder moment
66 during the forehand drive. Another study investigated the consequences of shoulder loadings
67 during forehand drive by estimating the distance between different shoulder structures
68 (Ladermann, Chague, Kolo, & Charbonnier, 2016). They observed a decrease in the humero-
69 glenoid distance that led, in 29% of the cases, to an anterior-superior humero-glenoid
70 impingement; namely an impingement of the deep surface of the subscapularis tendon and the
71 reflection pulley at the anterior-superior part of the glenoid cavity (Gerber & Sebesta, 2000).
72 Although these studies give a first estimation of the shoulder loadings during the forehand
73 drive, few information are available on the contact forces at the glenohumeral joint.

74 Contact forces take into consideration both the external forces and the muscle forces acting on
75 the joint (Steele, Demers, Schwartz, & Delp, 2012). Contact forces are usually hard to
76 estimate by experimental assessments since based on invasive methods such as instrumented
77 prosthesis (Nikooyan et al., 2010). Musculoskeletal models therefore offer a promising
78 alternative. Indeed, they make it possible to estimate muscle forces; then the later can be used

79 in addition to external forces to compute contact forces (Prinold, Masjedi, Johnson, & Bull,
80 2013; Quental, Folgado, Ambrosio, & Monteiro, 2015). Consequently, musculoskeletal
81 models have been already used to estimate glenohumeral contact forces during wheelchair
82 propulsion (Holloway et al., 2015; van Drongelen, van der Woude, & Veeger, 2011; Veeger,
83 Rozendaal, & van der Helm, 2002), driving task (Pandis, Prinold, & Bull, 2015) or daily life
84 activities (Anglin, Wyss, & Pichora, 2000). Consequently, musculoskeletal model may be
85 helpful to better assess glenohumeral contact forces during tennis forehand drives.

86 The aim of this study was to investigate the contact force at the glenohumeral joint during the
87 flat and topspin forehand drives in advanced tennis players. We hypothesised that contact
88 force magnitude and orientation would be similar for the flat and topspin forehand drives, and
89 different between the three phases of the stroke.

90

91 **Methods**

92 *Participants*

93 After given their informed consent, 11 right-handed male competitive tennis players (Mean \pm
94 SD age: 29.1 ± 7.6 years; mass: 69.4 ± 5.6 kg; height: 178 ± 6 cm; tennis experience: 22 ± 7
95 years; weekly training exposure: 5.1 ± 5.8 h; International Tennis Number: 3) volunteered to
96 participate in this study, which was approved by French Ethics Committee Sud-Est II. The
97 players declared no history of injury in the six months before the study. Six players used a
98 semi-western grip, while the other five a western grip, to hit forehand drive. All players were
99 classified in the advanced level (level 3) according to the International Tennis Number (ITN)
100 classification. This meant that the players were able to hit strong forehand drive with control,
101 depth and spin, and to vary spin. The mass, centre of gravity, swingweight and twistweight,
102 i.e. the moments of inertia around the transversal and perpendicular axis of the racket head
103 plane of each player were measured using a Racket Diagnostic Center (Babolat VS, Lyon,

104 France). Polar moment was calculated by subtracting the twistweight and swingweight
105 (Brody, 1985) (see Figure S1 in the supplementary file for axis definitions).

106

107 *Instrumentation and data collection*

108 In line with previous study (Rogowski, Creveaux, Cheze, Mace, & Dumas, 2014), each
109 participant was fitted with 17 reflective markers located on the xiphoid process; incisura
110 jugularis; 7th cervical vertebra; 8th thoracic vertebra; and on the right side, angulus
111 acromialis; acromio-clavicular joint; scapula spine (at 1/3 of the spine from the acromion);
112 inferior and superior scapula angles; distal insertion of the middle deltoid; medial and lateral
113 humeral epicondyles; olecranon; radial and ulnar styloid processes; and 2nd and 5th
114 metacarpal heads. In addition, three reflective markers were stuck on the racket and a
115 reflective tape surrounded the ball. The 3D trajectories of the reflective markers were
116 recorded using an optical motion capture system (Motion Analysis, Motion Analysis
117 Corporation, Santa Rosa, CA, USA) comprising eight digital cameras (sampling frequency:
118 500 Hz).

119

120 *Procedure*

121 After a 15-min warm-up, each player performed randomly two series of two sets of six
122 successive crosscourt forehand drives; flat forehand drives were hit during one series, and
123 topspin forehand drives during the second one. The players used their own racket (mass: 334
124 ± 13 g; centre of gravity measured from the handle racket extremity: 328 ± 8 mm;
125 swingweight: 327 ± 9 g.cm²; twistweight: 343 ± 10 g.cm²; polar moment: 15.7 ± 1 g.cm²).

126 They were instructed to hit the ball at their own playing velocity in a comfortable way, when
127 using a square stance. All trials were conducted in an indoor acrylic tennis court, which was
128 instrumented with a ball machine (ball velocity: 16.7 m/s; Airmatic 104, Pop-Lob, Bagneux,

129 France) located on the baseline of the opposite tennis court, and with a radar gun (Stalker Pro
130 II, Stalker Radar, Plano, TX, USA) located behind the player to measure ball velocity after the
131 ball impact.

132

133 *Musculoskeletal model*

134 The Delft Shoulder and Elbow model (van der Helm, 1994) available on OpenSim (Delp et
135 al., 2007) was used. Briefly, the model was composed of eight segments (ground, thorax, right
136 clavicle, scapula, humerus, ulna, radius and hand). A racket was added to the model to
137 reproduce the forehand drives. The segments were linked by 18 degrees of freedom namely
138 the ground-thorax joint (three translations and three rotations), sterno-clavicular joint (two
139 rotations), acromio-clavicular joint (three rotations), glenohumeral joint (three rotations),
140 elbow (two rotations) and wrist (two rotations). No degree of freedom was allowed between
141 the hand and the racket. The later was placed in the model for each participant according to its
142 position recorded at the beginning of the forehand drives. The 18 degrees of freedom were
143 actuated by 139 muscle lines of action (Figure 1).

144

145 *Scaling and kinematics*

146 The generic model was scaled for each participant using the position of the reflective markers
147 recorded during the static pose. In addition, the inertia, mass and size of the participants'
148 racket were used for each scaled model. Then, an inverse kinematic procedure was used to
149 obtain the joint angles by minimising the Euclidian distance between the position of the
150 virtual markers and the position of the experimental markers at each sample time. Moreover,
151 an ellipsoid fitted to the semi-right-thorax was implemented with a two-point-on-ellipsoid
152 constraint ensuring the scapula to follow the thoracic curvature throughout the movement
153 (Michaud, 2016, July). For further analysis, joint angles were filtered using a zero-lag fourth-

154 order low-pass Butterworth filter with an 8 Hz cut-off frequency. To avoid problems of data
 155 filtering through ball impact (Knudson & Bahamonde, 2001), three frames around the ball
 156 impact (determined according to Creveaux et al. (2013b)) were deleted; then the data were
 157 filtered separately before and after the ball impact.

158

159 *Glenohumeral contact forces*

160 The joint kinematics and scaled models were used as input of the static optimisation
 161 procedure (Delp et al., 2007) in order to obtain muscle activations required to perform the
 162 forehand drives. Briefly, at each sample time (t), the objective function (J) to minimise
 163 consisted in the quadratic sum of muscle activations (a) and the quadratic sum of residual
 164 torques (i.e. artificial joint actuators used to solve the numerical problem when muscles
 165 cannot reproduce the joint torque computed with inverse dynamics procedure) (τ^{res}) at each
 166 degree of freedom (n), subject to two constraints 1) the joint torques calculated from muscle
 167 activations were equal to the torques (τ) computed from the inverse dynamic procedure
 168 (Eq. 2) and 2) the glenohumeral forces were inside a friction polygon ensuring the stability of
 169 the glenohumeral joint (Eq. 3) (Dickerson, Chaffin, & Hughes, 2007).

170

$$\min_{a(t)_m} J(t) = c_1 * \sum_{m=1}^{139} (a(t)_m)^2 + c_2 * \sum_{n=1}^{18} (\tau^{res}(t)_n)^2 , \quad (\text{Eq. 1})$$

171 *subject to*

$$\sum_{m=1}^{139} r_{m,j} \cdot [a(t)_m \cdot f(F_m^0, l_m, v_m)] + \sum_{n=1}^{18} \tau^{res}(t)_n = \tau(t)_j , \quad (\text{Eq. 2})$$

$$\begin{bmatrix} \alpha_1\mu_1 & -1 & 0 \\ \alpha_2\mu_2 & -1 & -1 \\ \alpha_3\mu_3 & 0 & -1 \\ \alpha_4\mu_4 & 1 & -1 \\ \alpha_5\mu_5 & 1 & 0 \\ \alpha_6\mu_6 & 1 & 1 \\ \alpha_7\mu_7 & 0 & 1 \\ \alpha_8\mu_8 & -1 & 1 \end{bmatrix} \cdot \begin{bmatrix} R_{GH}^n \\ R_{GH}^{s1} \\ R_{GH}^{s2} \end{bmatrix} \geq \mathbf{0} \quad , \quad (\text{Eq. 3})$$

172 with m referring to the 139 muscle-tendon-units; F_m^0 is the maximum isometric force of the
 173 modelled muscles m ; l_m is the muscle model length; v_m denotes the muscle model
 174 shortening/lengthening velocity; $f(F_m^0, l_m, v_m)$ is its force-length-velocity surface
 175 relationship; $r_{m,j}$ is the moment arm about j^{th} joint axis; c_1 and c_2 referring to weighting
 176 factors; $R_{GH}^n, R_{GH}^{s1}, R_{GH}^{s2}$: the normal, posterior-anterior and superior-inferior glenohumeral
 177 contact force components; μ_i : the dislocation thresholds equal to [0.29, 0.33, 0.51, 0.35, 0.30,
 178 0.43, 0.56, 0.4] (Dickerson et al., 2007) for each polygon vertex (i), α_i : optimised coefficients
 179 (Wieber, 2001) to best match with Dickerson's polygon (2007).

180 The glenohumeral contact forces between the humeral head and scapula \vec{R}_{GH} were
 181 calculated using the *jointReaction* algorithm of OpenSim 3.2 (Delp et al., 2007; Steele et al.,
 182 2012):

$$\vec{R}_{GH} = [M]_{\text{humerus}} \cdot \vec{a}_{\text{humerus}} - \left(\vec{R}_{\text{elbow}} + \sum \vec{F}_{\text{muscles}} + \vec{F}_{\text{gravity}} \right), \quad (\text{Eq. 4})$$

183 $[M]_{\text{humerus}}$ is the matrix of inertial properties of the humerus, \vec{a}_{humerus} denotes the six
 184 dimensional angular and linear accelerations of the humerus, \vec{R}_{elbow} is the force and moment
 185 of the ulna on the humerus; \vec{F}_{muscles} and \vec{F}_{gravity} are the muscle and gravitational forces and
 186 moments acting on the humerus. Glenohumeral contact forces were initially calculated in the
 187 scapula reference system. In order to express these forces in the glenoid reference system,
 188 three landmarks were located on the scapula of the generic Opensim model (most anterior,
 189 posterior and inferior points of the edge of the glenoid). These landmarks were used to define

190 the reference system of the glenoid. Finally, the transformation matrix scapula-to-glenoid was
191 used to compute glenohumeral contact forces in the glenoid reference system.

192

193 *Analysis*

194 Among all forehand drives performed, only the three for which the ball bounced in the
195 opposite court and with similar ball post-impact velocities were taken into consideration in the
196 subsequent analysis. Four key-events were detected, such as the beginning of the shoulder
197 turn, first forward movement of the racket, ball impact, and highest elbow height after impact
198 (Ryu et al., 1988), in order to define three successive phases: (1) the backswing; (2) the
199 forward swing and (3) the follow-through.

200 For each phase, the mean and maximal values of the compressive, shearing and total
201 glenohumeral contact forces were calculated. In line with a previous study (Charbonnier et al.,
202 2015), the direction of the glenohumeral contact forces was expressed by dividing the glenoid
203 into eight sections (Figure 2). Then, the percentage of glenohumeral contact forces inside each
204 of the eight sections was computed. Finally, for each variable cited above, the values obtained
205 either for the flat or topspin forehand drives were averaged separately, in order to obtain one
206 value per variable and per forehand drive technique.

207 In order to evaluate the model outputs, mean and maximal residual torques were computed
208 and compared to the joint torques calculated by the inverse dynamic procedure. In addition,
209 the mean activation of nine muscles (anterior, middle, posterior deltoids; pectoralis major;
210 latissimus dorsi; serratus anterior; infraspinatus; supraspinatus and subscapularis) was
211 calculated and ranked by order of intensity to be compared with EMG data from the literature.
212 The rank comparison was chosen instead of the comparison of activation values since
213 musculoskeletal model activations are different from experimental normalised EMG.

214

215 *Statistical analysis*

216 The interaction effect between the forehand drive technique (flat vs. topspin; fixed effect) and
217 the phase (backswing vs. forward swing vs. follow-through; fixed effect) on the mean and
218 maximal compressive, shearing and total glenohumeral contact forces was tested using linear
219 mixed models. Linear mixed-model is an alternative method to the ANOVA on repeated
220 measures that may be more advantageous especially with categorical data (Barr, Levy,
221 Scheepers, & Tily, 2013). As within-participants repeated measures were performed,
222 participants were entered as random intercept. To avoid the effect of a different racket
223 velocity at the frame before the impact between the flat and topspin forehand drives, the
224 racket velocity was also entered as random intercept. Finally, as the forehand drive technique
225 might have different effect with respect to the participants and/or the racket velocity, forehand
226 drive technique was also entered as random slope (Barr et al., 2013). The p -values were
227 obtained by likelihood ratio tests of the full model against the model without the effect in
228 question. The level of significance was set at $p < 0.008$ (Bonferroni correction $0.05/6$
229 variables). When a main effect was revealed by the linear mixed-model, post-hoc pairwise
230 comparisons were performed using the Tukey's honestly significant difference procedure with
231 a significant p -value set at 0.05. The linearity, homoscedasticity and normality of the linear-
232 mixed model residuals were graphically controlled. All models were performed using the
233 package *lme4* of R software (R 3.2, RCore Team 2014, Vienna, Austria).

234 The chi-square test of independence was used to assess if the proportion of glenohumeral
235 contact forces inside the eight glenoid sections was dependent of the forehand drive
236 technique. Finally, the difference in the proportion of glenohumeral contact forces between
237 each glenoid section was tested using the chi-square test for homogeneity of proportion. All
238 chi-square tests were executed using R software.

239

240 **Results**

241 *Evaluation of the model outputs*

242 Regardless the forehand drive technique, the maximal residual torques were on average $14.7 \pm$
243 2.3 , 8.4 ± 4.9 and 22.6 ± 7.2 times smaller than the corresponding maximal joint torques for
244 the sterno-clavicular, acromio-clavicular and glenohumeral joint respectively. Greater
245 differences were observed concerning the mean residual torques which were in average $29.7 \pm$
246 7.1 , 14.3 ± 6.8 and 37.6 ± 10.5 times smaller than the corresponding mean joint torques for
247 the sterno-clavicular, acromio-clavicular and glenohumeral joint, respectively.

248 The qualitative analysis of the muscle activations enabled to point out low activations for all
249 muscles during the backswing phase (Figure 3). The pectoralis major/minor, anterior deltoid,
250 subscapularis and upper trapezius were highly activated in comparison to the other shoulder
251 muscles during the forward swing phase (Figure 3). Finally, the middle and posterior deltoids,
252 latissimus dorsi, infraspinatus, upper and middle trapezius were mainly involved during the
253 follow-through phase. The ranking order of muscle mean activation between phases was
254 overall similar to those reported by Ryu et al. (1988) (Table 1).

255

256 *Forehand drive analysis*

257 The mean ball velocities were 31.5 ± 5.5 m/s for flat and 27.4 ± 4.6 m/s for the topspin
258 forehand drives. The norms of the 3D racket velocity one frame before the impact were on
259 average 20.2 ± 4.5 m/s for flat and 21.7 ± 5.3 m/s for the topspin forehand drives. Finally, the
260 mean racket vertical velocities were 6.6 ± 2.1 m/s for flat and 11.1 ± 1.9 m/s for the topspin
261 forehand drives.

262 The linear mixed models revealed only a main effect of the phase on the mean and maximal
263 compressive, shearing and total glenohumeral contact forces ($\chi^2(2) \in [68.7, 87]$, $p < 0.001$). The
264 glenohumeral contact forces during the forward swing phase were in average 1.25 time

265 greater than during the follow-through phase, and 5.8 times greater than during the backswing
266 phase (Table 2 and figure 4).

267 Concerning the repartition of the glenohumeral contact forces in the eight glenoid sections,
268 the chi-square test of independence revealed no dependency between the forehand drive
269 technique and the glenoid sections either for the backswing ($\chi^2(7)=0.34$, $p=0.99$), forward
270 swing ($\chi^2(7)=2.41$, $p=0.93$) or follow-through phases ($\chi^2(7)=8.59$, $p=0.28$). Regardless the
271 forehand drive technique, the chi-square test for homogeneity revealed for each phase that the
272 distribution of the glenohumeral contact forces in the sections of the glenoid was not
273 homogeneous ($\chi^2(7)=462$, $p<0.001$; $\chi^2(7)=440$, $p<0.001$; $\chi^2(7)=167$, $p<0.001$, respectively for
274 the backswing, forward swing and follow-through phases). For the backswing and forward
275 swing phases, the greatest residual of the chi-square tests was observed for the
276 “anteriorSuperior” section (Figure 2), while concerning the follow-through phase, the greatest
277 residual of the chi-square tests was observed for the “superiorAnterior” section (see Table T1
278 of the residuals in the supplementary file).

279

280 **Discussion and implications**

281 This study aimed to investigate the contact forces at the glenohumeral joint during the flat and
282 topspin forehand drives in advanced tennis players. The first findings were that the forehand
283 drive technique, i.e. flat or topspin, did not change the glenohumeral contact forces undergone
284 by the tennis player. The second findings were that the maximal contact force undergone by
285 the glenohumeral joint occurred during the forward swing phase, and pointed toward the
286 anterior-superior part of the glenoid.

287

288 *Evaluation of the model outputs*

289 As the computed glenohumeral contact forces resulted from the modelled muscle forces, the
290 validity of our model needed to be evaluated. The values for the maximal and mean residual
291 torques involved during the forehand drive motion were between 8.4 and 37.6 times smaller
292 than the maximal and mean torques computed with the inverse dynamic procedure. These
293 results meant that the muscles included in the model were sufficient to ensure the joint torques
294 necessary to perform the forehand drives (Hicks, Uchida, Seth, Rajagopal, & Delp, 2015).
295 Regardless the forehand drive technique, the orders of the magnitude of muscle activations
296 between phases was similar than the normalised EMG data of Ryu et al. (1988). Only three
297 muscles had a different ranking, namely the infraspinatus, supraspinatus and middle deltoid
298 muscles (Table 1). The mean normalised EMG levels of these muscles however present small
299 differences between the phases of the forehand drive, i.e. 3 to 11% (Ryu et al., 1988),
300 potentially explaining the discrepancies in the rank between studies. The changes in racket
301 specifications over the last 30 years may also result in differences in player's motion, and then
302 in muscle demand, hence explaining some of the discrepancies between the two studies. In
303 comparison with Genevois, Creveaux, Hautier, and Rogowski (2015) and Rota, Morel,
304 Saboul, Rogowski, and Hautier (2014), we also observed that the mean activations of the
305 anterior deltoid and pectoralis major were greater than the mean activations of the latissimus
306 dorsi and middle deltoid (Figure 3).
307 In summary, our model seemed to respect the salient characteristic of the forehand drive
308 performed by the players. Although our computed glenohumeral contact forces could not be
309 compared with in-vivo data (see limitations section), we assume that they were suitable for
310 further interpretation.

311

312 *Glenohumeral contact forces*

313 The contribution of the shoulder complex to the racket velocity production remains similar
314 whatever the technique required to hit a forehand drive (Takahashi et al., 1996). This outcome
315 may partly explain the lack of differences in the glenohumeral contact forces computed during
316 both the flat and topspin forehand drives. It is also possible that our model was not
317 sufficiently accurate to detect the small changes in glenohumeral contact forces with respect
318 to the forehand drive technique. Grouping the results for both techniques of shots nevertheless
319 provided new information on the glenohumeral contact forces during the tennis forehand
320 drive.

321 The achievement of a forehand drive requires firstly a slow motion, then a rapid acceleration,
322 and finally a deceleration of the upper limb – racket complex (Elliott & Marsh, 1989). Such a
323 motion pattern may explain the differences observed in maximal glenohumeral contact forces
324 between the three phases, e.g. 559 ± 145 N, 3573 ± 1383 N and 2327 ± 1162 N, for the
325 backswing, forward swing and follow-through phase respectively. These results suggested
326 that the player's shoulder was not at the same level of risk for injury throughout the forehand
327 drive motion. During the backswing phase, a trunk rotation occurs to place it perpendicularly
328 to the net (Elliott & Marsh, 1989), while the humerus abducts, extends, and externally rotates
329 to take back the racket. The activation of the teres minor muscle may contribute to place the
330 humerus in the adequate position at the end of the backswing, whereas the pectoralis minor
331 muscle mainly acts to anteriorly tilt the scapula (Rogowski, Creveaux, Cheze, & Dumas,
332 2014) (Figure 3). The anterior and superior orientation of the glenohumeral contact forces
333 may be partly related to the early activation of the anterior deltoid muscle, which is involved
334 in the stretch-shorten cycle movement to contribute to a powerful shot (Wilson, Elliott, &
335 Wood, 1991). As the positioning of the racket at the end of the backswing phase requires low
336 muscle activations, the shearing forces and consequently the compressive forces (that ensure
337 the glenohumeral stability) remained at low levels. During the forward swing phase, a large

338 demand is placed on the pectoralis major/minor, anterior deltoid and subscapularis muscles to
339 achieve a rapid humeral horizontal adduction and internal rotation (Figure 3) (Ryu et al.,
340 1988). As these muscles cross the glenohumeral joint, their increased activation automatically
341 led to raise the compressive and shearing glenohumeral contact forces and to orientate them
342 toward the anterior section of the glenoid. It may be hypothesised that the activation of the
343 latissimus dorsi, teres minor, infraspinatus, and rhomboid became crucial to counteract the
344 increased shearing glenohumeral force. Their activation may have contributed to the increased
345 compressive glenohumeral force, ensuring then the glenohumeral stability (Dickerson et al.,
346 2007; Lippitt & Matsen, 1993). During the follow-through phase, the glenohumeral contact
347 forces decreased, even if they remained relatively high in comparison to the backswing phase.
348 This may be explained by the high velocity of the arm during the follow-through phase
349 (Marshall & Elliott, 2000). The middle deltoid and upper trapezius were involved in the
350 humeral abduction, and may contribute to upwardly orientate the glenohumeral contact forces.
351 The middle trapezius, infraspinatus, teres minor and posterior deltoid muscles then may
352 contract eccentrically to resist to the anterior glenohumeral shearing forces. Although our
353 model did not allow translations of the humeral head, the observation of the orientation of the
354 glenohumeral contact forces leads to the same conclusions than Ladermann et al. (2016). The
355 muscle forces produced during the forehand drive result in glenohumeral contact forces
356 pointing in a forward and upward direction; the consequence may be a translation of the
357 humeral head that may cause an anterior-superior humero-glenoid impingement.

358

359 *Limitations*

360 The first limitation of this study was that the glenohumeral contact forces were estimated and
361 not measured in-vivo. Nevertheless, only invasive methods make possible to measure
362 glenohumeral contact forces. To the best of our knowledge, few studies measured in-vivo

363 glenohumeral contact forces, only focusing on arm elevation, isometric forces (Nikooyan et
364 al., 2010) and daily living activities (Westerhoff et al., 2009, 2012), but not during sport
365 movements. In addition, to our knowledge, glenohumeral contact forces estimated through
366 musculoskeletal model were only investigated during wheelchair tasks (Holloway et al., 2015;
367 van der Helm & Veeger, 1996; van Drongelen et al., 2011), but not for sport movements.
368 Although the comparison between our results and the previous studies is not obvious, our
369 computed contact forces (Table 2) were up to four times greater than the maximal
370 glenohumeral forces measured in-vivo with an instrumented prosthesis during arm elevation
371 (≈ 800 N.) (Nikooyan et al., 2010). In comparison to other musculoskeletal models, we found
372 glenohumeral contact forces in the same range than those estimated during wheelchair
373 propulsion (Holloway et al., 2015; van der Helm & Veeger, 1996) or during vertical weight
374 relief lift from a wheelchair (van Drongelen et al., 2011). Consequently, the values of the
375 glenohumeral contact forces obtained in this study must be taken with caution even if they do
376 not seem to be abnormal in comparison to the literature.

377 The second limitation was that our model enabled only three rotations at the glenohumeral
378 joint and no translation. Although the computing of the glenohumeral contact forces is
379 probably affected by the number of degrees of freedom, the orientation of the glenohumeral
380 contact forces calculated in our study led to similar conclusions than those of Ladermann et
381 al. (2016) who had implemented glenohumeral translation in their kinematic model. In
382 addition, our kinematical model obtained only from skin markers did not enable to estimate
383 accurately the very small glenohumeral translations occurring during forehand drives (less
384 than 2.8 mm for forehand drive mimic) (Dal Maso et al., 2015). The third limitation of our
385 study was that the muscle forces of the model were not specific to those of the participants. It
386 may be possible that the tennis players of this study had different maximal isometric muscle
387 forces than those implemented in the generic Delft Shoulder and Elbow model. Further

388 studies are needed with participant-specific musculoskeletal model to estimate more precisely
389 glenohumeral contact forces.

390

391 **Conclusion**

392 This study was the first to estimate glenohumeral contact forces during forehand drives,
393 through musculoskeletal modelling. Regardless the forehand drive technique (flat or topspin),
394 the tennis players underwent the greatest glenohumeral contact forces during the forward
395 swing, then during the follow-through and finally during the backswing phase. Most of the
396 glenohumeral contact forces pointed toward the anterior-superior part of the glenoid. This
397 study brings new knowledge on the glenohumeral loadings during real sport motion, and
398 provides information that may help the sport clinicians and tennis coaches on the causative
399 factors for shoulder problems.

400

401 **References**

- 402 Anglin, C., Wyss, U. P., & Pichora, D. R. (2000). Glenohumeral contact forces. *Proceedings*
403 *of the Institution of Mechanical Engineers. Part H, Journal of Engineering in Medicine,*
404 *214, 637-644. doi: 10.1243/0954411001535660*
- 405 Bahamonde, R. E., & Knudson, D. (2003). Kinetics of the upper extremity in the open and
406 square stance tennis forehand. *Journal of Science and Medicine in Sport, 6, 88-101. doi:*
407 *10.1016/S1440-2440(03)80012-9*
- 408 Barr, D. J., Levy, R., Scheepers, C., & Tily, H. J. (2013). Random effects structure for
409 confirmatory hypothesis testing: Keep it maximal. *Journal of Memory and Language,*
410 *68, 255-278. doi: 10.1016/j.jml.2012.11.001*
- 411 Charbonnier, C., Chague, S., Kolo, F. C., & Ladermann, A. (2015). Shoulder motion during
412 tennis serve: dynamic and radiological evaluation based on motion capture and
413 magnetic resonance imaging. *International Journal of Computer Assisted Radiology*
414 *and Surgery, 10, 1289-1297. doi: 10.1007/s11548-014-1135-4*

415 Creveaux, T., Dumas, R., Cheze, L., Mace, P., & Rogowski, I. (2013a). Influence of racket
416 polar moment on joint loads during tennis forehand drive. *Computer Methods in*
417 *Biomechanics and Biomedical Engineering*, *16 Suppl 1*, 99-101. doi:
418 10.1080/10255842.2013.815922

419 Creveaux, T., Dumas, R., Hautier, C., Mace, P., Cheze, L., & Rogowski, I. (2013b). Joint
420 Kinetics to Assess the Influence of the Racket on a Tennis Player's Shoulder. *Journal of*
421 *Sports Science & Medicine*, *12*, 259-266. Retrieve from
422 <http://www.jssm.org/researchjssm-12-259.xml.xml>

423 Dal Maso, F., Raison, M., Lundberg, A., Arndt, A., Allard, P., & Begon, M. (2015).
424 Glenohumeral translations during range-of-motion movements, activities of daily living,
425 and sports activities in healthy participants. *Clinical Biomechanics*, *30*, 1002-1007. doi:
426 10.1016/j.clinbiomech.2015.06.016

427 Delp, S. L., Anderson, F. C., Arnold, A. S., Loan, P., Habib, A., John, C. T., . . . Thelen, D. G.
428 (2007). OpenSim: open-source software to create and analyze dynamic simulations of
429 movement. *IEEE Transactions on Bio-medical Engineering*, *54*, 1940-1950. doi:
430 10.1109/TBME.2007.901024

431 Dickerson, C. R., Chaffin, D. B., & Hughes, R. E. (2007). A mathematical musculoskeletal
432 shoulder model for proactive ergonomic analysis. *Computer Methods in Biomechanics*
433 *and Biomedical Engineering*, *10*, 389-400. doi: 10.1080/10255840701592727

434 Elliott, B., Fleisig, G., Nicholls, R., & Escamilia, R. (2003). Technique effects on upper limb
435 loading in the tennis serve. *Journal of Science and Medicine in Sport*, *6*, 76-87. doi:
436 10.1016/S1440-2440(03)80011-7

437 Elliott, B., & Marsh, T. (1989). A biomechanical comparison of the topspin and backspin
438 forehand approach shots in tennis. *Journal of Sports Sciences*, *7*, 215-227. doi:
439 10.1080/02640418908729842

440 Genevois, C., Creveaux, T., Hautier, C., & Rogowski, I. (2015). Trunk and Shoulder Muscle
441 Coordination during One, Two-Handed Medicine-Ball Side Throws and Tennis
442 Forehand Drive. *Journal of Athletic Enhancement*, *4*, 1-6. doi: 10.4172/2324-
443 9080.1000201

444 Gerber, C., & Sebesta, A. (2000). Impingement of the deep surface of the subscapularis
445 tendon and the reflection pulley on the anterosuperior glenoid rim: a preliminary report.
446 *Journal of Shoulder and Elbow Surgery*, *9*, 483-490. doi: 10.1067/mse.2000.109322

447 Hicks, J. L., Uchida, T. K., Seth, A., Rajagopal, A., & Delp, S. L. (2015). Is my model good
448 enough? Best practices for verification and validation of musculoskeletal models and

449 simulations of movement. *Journal of Biomechanical Engineering*, 137, 020905. doi:
450 10.1115/1.4029304

451 Holloway, C. S., Symonds, A., Suzuki, T., Gall, A., Smitham, P., & Taylor, S. (2015).
452 Linking wheelchair kinetics to glenohumeral joint demand during everyday accessibility
453 activities. *Conference Proceedings IEEE Engineering in Medicine and Biology Society,*
454 *2015*, 2478-2481. doi: 10.1109/EMBC.2015.7318896

455 Knudson, D., & Bahamonde, R. (2001). Effect of endpoint conditions on position and velocity
456 near impact in tennis. *Journal of Sports Sciences*, 19, 839-844. doi:
457 10.1080/026404101753113787

458 Ladermann, A., Chague, S., Kolo, F. C., & Charbonnier, C. (2016). Kinematics of the
459 shoulder joint in tennis players. *Journal of Science and Medicine in Sport*, 19, 56-63.
460 doi: 10.1016/j.jsams.2014.11.009

461 Landlinger, J., Lindinger, S. J., Stoggl, T., Wagner, H., & Muller, E. (2010). Kinematic
462 differences of elite and high-performance tennis players in the cross court and down the
463 line forehand. *Sports Biomechanics*, 9, 280-295. doi: 10.1080/14763141.2010.535841

464 Lippitt, S., & Matsen, F. (1993). Mechanisms of glenohumeral joint stability. *Clinical*
465 *Orthopaedics and Related Research*, 20-28. doi: 10.1097/00003086-199306000-00004

466 Marshall, R. N., & Elliott, B. C. (2000). Long-axis rotation: the missing link in proximal-to-
467 distal segmental sequencing. *Journal of Sports Sciences*, 18, 247-254. doi:
468 10.1080/026404100364983

469 Michaud, B. (2016, July). *Thorax ellipsoid optimization based on scapula movements' area*
470 *improves kinematic reconstruction of the scapula*. Paper presented at the meeting of
471 Digital Human Modeling Congress, Montreal Canada.

472 Nikooyan, A. A., Veeger, H. E., Westerhoff, P., Graichen, F., Bergmann, G., & van der Helm,
473 F. C. (2010). Validation of the Delft Shoulder and Elbow Model using in-vivo
474 glenohumeral joint contact forces. *Journal of Biomechanics*, 43, 3007-3014. doi:
475 10.1016/j.jbiomech.2010.06.015

476 Pandis, P., Prinold, J. A., & Bull, A. M. (2015). Shoulder muscle forces during driving:
477 Sudden steering can load the rotator cuff beyond its repair limit. *Clinical Biomechanics*,
478 30, 839-846. doi: 10.1016/j.clinbiomech.2015.06.004

479 Prinold, J. A., Masjedi, M., Johnson, G. R., & Bull, A. M. (2013). Musculoskeletal shoulder
480 models: a technical review and proposals for research foci. *Proceedings of the*
481 *Institution of Mechanical Engineers. Part H, Journal of Engineering in Medicine*, 227,
482 1041-1057. doi: 10.1177/0954411913492303

- 483 Quental, C., Folgado, J., Ambrosio, J., & Monteiro, J. (2015). Critical analysis of
484 musculoskeletal modelling complexity in multibody biomechanical models of the upper
485 limb. *Computer Methods in Biomechanics and Biomedical Engineering*, *18*, 749-759.
486 doi: 10.1080/10255842.2013.845879
- 487 Rogowski, I., Creveaux, T., Cheze, L., & Dumas, R. (2014). Scapulothoracic kinematics
488 during tennis forehand drive. *Sports Biomechanics*, *13*, 166-175. doi:
489 10.1080/14763141.2014.885073
- 490 Rogowski, I., Creveaux, T., Cheze, L., Mace, P., & Dumas, R. (2014). Effects of the racket
491 polar moment of inertia on dominant upper limb joint moments during tennis serve.
492 *PloS One*, *9*, e104785. doi: 10.1371/journal.pone.0104785
- 493 Rota, S., Morel, B., Saboul, D., Rogowski, I., & Hautier, C. (2014). Influence of fatigue on
494 upper limb muscle activity and performance in tennis. *Journal of Electromyography and*
495 *Kinesiology*, *24*, 90-97. doi: 10.1016/j.jelekin.2013.10.007
- 496 Ryu, R. K., McCormick, J., Jobe, F. W., Moynes, D. R., & Antonelli, D. J. (1988). An
497 electromyographic analysis of shoulder function in tennis players. *The American*
498 *Journal of Sports Medicine*, *16*, 481-485. doi: 10.1177/036354658801600509
- 499 Seeley, M. K., Funk, M. D., Denning, W. M., Hager, R. L., & Hopkins, J. T. (2011). Tennis
500 forehand kinematics change as post-impact ball speed is altered. *Sports Biomechanics*,
501 *10*, 415-426. doi: 10.1080/14763141.2011.629305
- 502 Steele, K. M., Demers, M. S., Schwartz, M. H., & Delp, S. L. (2012). Compressive
503 tibiofemoral force during crouch gait. *Gait & Posture*, *35*, 556-560. doi:
504 10.1016/j.gaitpost.2011.11.023
- 505 Takahashi, K., Elliott, B., & Noffal, G. (1996). The role of upper limb segment rotations in
506 the development of spin in the tennis forehand. *Australian Journal of Science and*
507 *Medicine in Sport*, *28*, 106-113. Retrieve from
508 <http://europepmc.org/abstract/med/9040900>
- 509 van der Helm, F. C. (1994). A finite element musculoskeletal model of the shoulder
510 mechanism. *Journal of Biomechanics*, *27*, 551-569. doi: 10.1016/0021-9290(94)90065-
511 5
- 512 van der Helm, F. C., & Veeger, H. E. (1996). Quasi-static analysis of muscle forces in the
513 shoulder mechanism during wheelchair propulsion. *Journal of Biomechanics*, *29*, 39-52.
514 doi: 10.1016/0021-9290(95)00026-7

- 515 van Drongelen, S., van der Woude, L. H., & Veeger, H. E. (2011). Load on the shoulder
516 complex during wheelchair propulsion and weight relief lifting. *Clinical Biomechanics*,
517 26, 452-457. doi: 10.1016/j.clinbiomech.2011.01.006
- 518 Veeger, H. E., Rozendaal, L. A., & van der Helm, F. C. (2002). Load on the shoulder in low
519 intensity wheelchair propulsion. *Clinical Biomechanics*, 17, 211-218. doi:
520 10.1016/S0268-0033(02)00008-6
- 521 Westerhoff, P., Graichen, F., Bender, A., Halder, A., Beier, A., Rohlmann, A., & Bergmann,
522 G. (2009). In vivo measurement of shoulder joint loads during activities of daily living.
523 *Journal of Biomechanics*, 42, 1840-1849. doi: 10.1016/j.jbiomech.2009.05.035
- 524 Westerhoff, P., Graichen, F., Bender, A., Halder, A., Beier, A., Rohlmann, A., & Bergmann,
525 G. (2012). In vivo measurement of shoulder joint loads during walking with crutches.
526 *Clinical Biomechanics*, 27, 711-718. doi: 10.1016/j.clinbiomech.2012.03.004
- 527 Wilson, G. J., Elliott, B. C., & Wood, G. A. (1991). The effect on performance of imposing a
528 delay during a stretch-shorten cycle movement. *Medicine and Science in Sports and*
529 *Exercise*, 23, 364-370. doi: 10.1249/00005768-199103000-00016

530

531

532 **Table 1.** Ranked order between phases by intensity of muscle activations or normalised EMG
 533 for seven shoulder muscles in comparison to the data of Ryu et al. (1988). The greater the
 534 rank, the greater the activation intensity or normalised EMG.

		Backswing	Forward swing	Follow-through
Pectoralis Major	Ryu (1988)	1	3	2
	Our model	1	3	2
Latissimus dorsi	Ryu (1988)	1	2	3
	Our model	1	2	3
Serratus Anterior	Ryu (1988)	1	3	2
	Our model	1	3	2
Middle deltoid	Ryu (1988)	3	1	2
	Our model	1*	2*	3*
Infraspinatus	Ryu (1988)	2	1	3
	Our model	1*	2*	3
Supraspinatus	Ryu (1988)	2	3	1
	Our model	1*	2*	3*
Subscapularis	Ryu (1988)	1	3	2
	Our model	1	3	2

535 * *denotes a difference in rank order between our model and Ryu's data.*

536

537 **Table 2.** Mean \pm standard deviation of the mean and maximal compressive, shearing and total
 538 glenohumeral forces with respect to the phase (backswing, forward swing and follow-
 539 through). As no effect of the forehand drive technique has been observed, values for the flat
 540 and topspin forehand drives were averaged.

	Backswing	Forward swing	Follow-through	p-values
Maximal				
Compressive (N)	530 \pm 137	3396 \pm 1323	2210 \pm 1103	***, ##, †††
Shear (N)	176 \pm 49	1116 \pm 410	754 \pm 361	***, ##, †††
Total (N)	559 \pm 145	3573 \pm 1383	2327 \pm 1162	***, ##, †††
Mean				
Compressive (N)	262 \pm 65	1513 \pm 643	1215 \pm 596	***, †, †††
Shear (N)	87 \pm 23	498 \pm 211	394 \pm 221	***, †, †††
Total (N)	276 \pm 69	1593 \pm 677	1281 \pm 633	***, †, †††

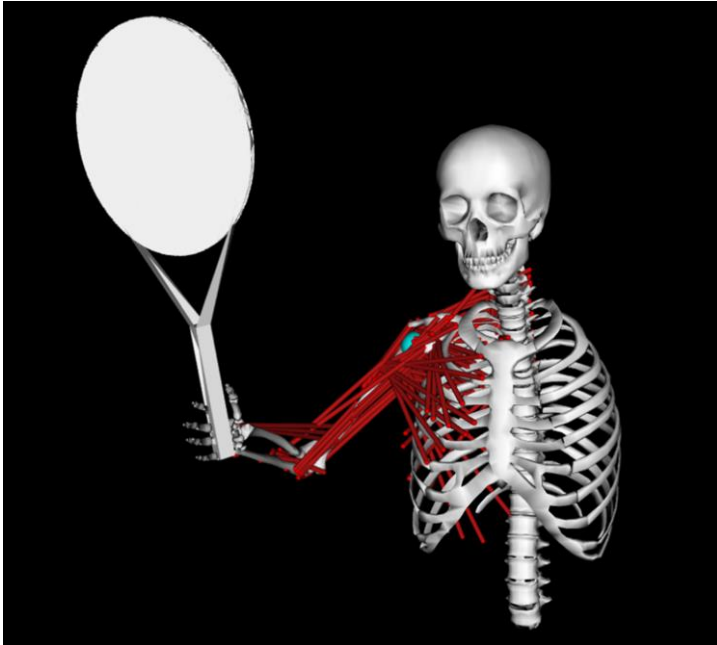
541 * indicates a significant difference between the backswing and forward swing phases (* for
 542 p<0.05; ** for p<0.01; *** for p<0.001); † indicates a significant difference between the
 543 forward swing and follow-through phases († for p<0.05; # for p<0.01; ## for p<0.001); ‡
 544 indicates a significant difference between the backswing and follow-through phases (‡ for
 545 p<0.05; †† for p<0.01; ††† for p<0.001).

546
 547
 548
 549
 550

551

552 **Figure 1.** Delft Shoulder and Elbow model implemented with a tennis racket

553

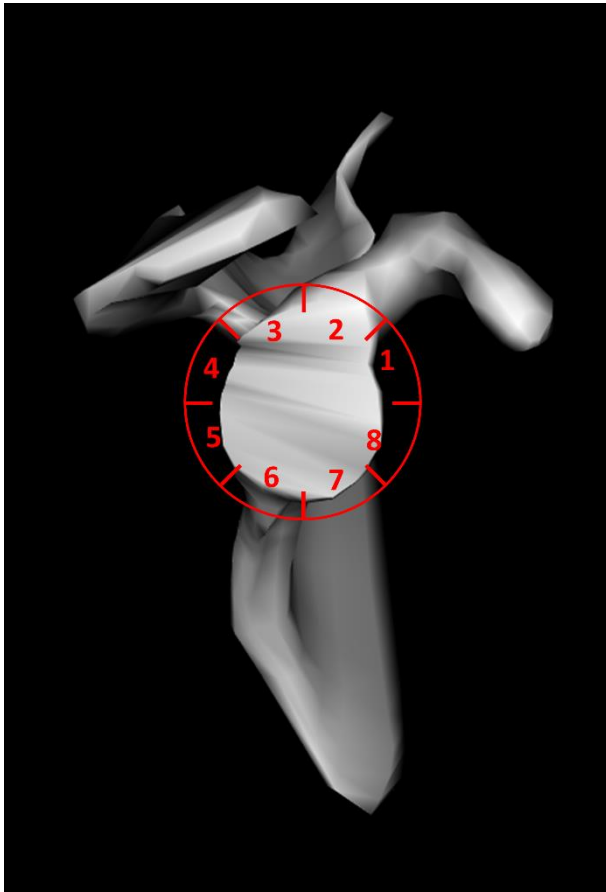


554

555

556

557 **Figure 2.** The glenoid was divided into eight sectors based on Charbonnier et al. (2015) in
558 order to represent the direction of the glenohumeral forces: 1-anteriorSuperior, 2-
559 superiorAnterior, 3-superiorPosterior, 4-posteriorSuperior, 5-posteriorInferior, 6-
560 inferiorPosterior, 7-inferiorAnterior and 8-anteriorInferior

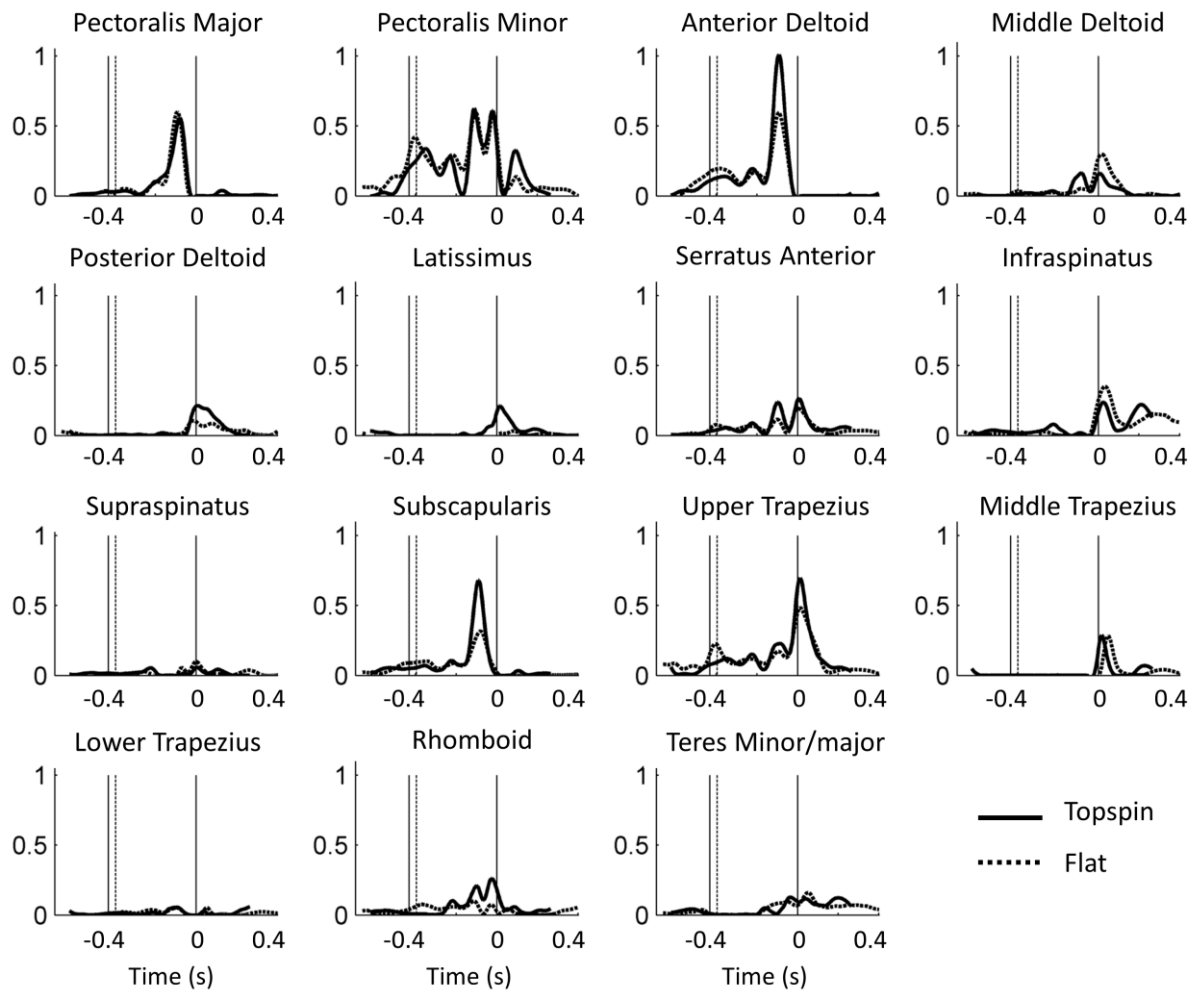


561

562

563

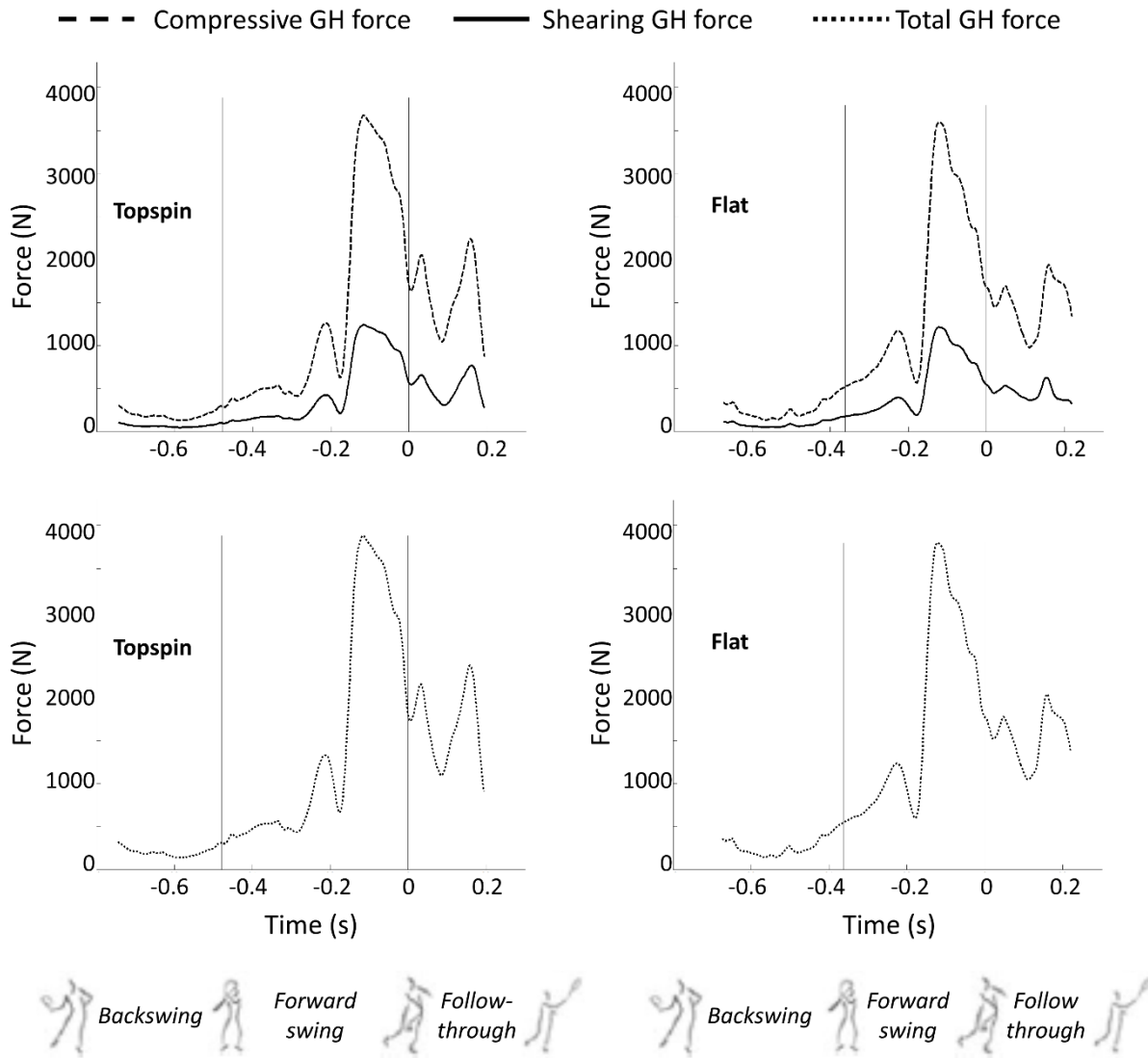
564 **Figure 3.** Muscle activations of a representative participant obtained with the musculoskeletal
 565 model. Zero second fits the ball impact. The vertical dashed and solid black lines correspond
 566 to the beginning of the forward swing phase for the flat and topspin forehand drives
 567 respectively.



568

569

570 **Figure 4.** Compressive (dashed line), shearing (solid line) and total (dotted line)
 571 glenohumeral (GH) forces during the flat and topspin forehand drives of a representative
 572 participant with respect to the time. Zero second fits the ball impact.

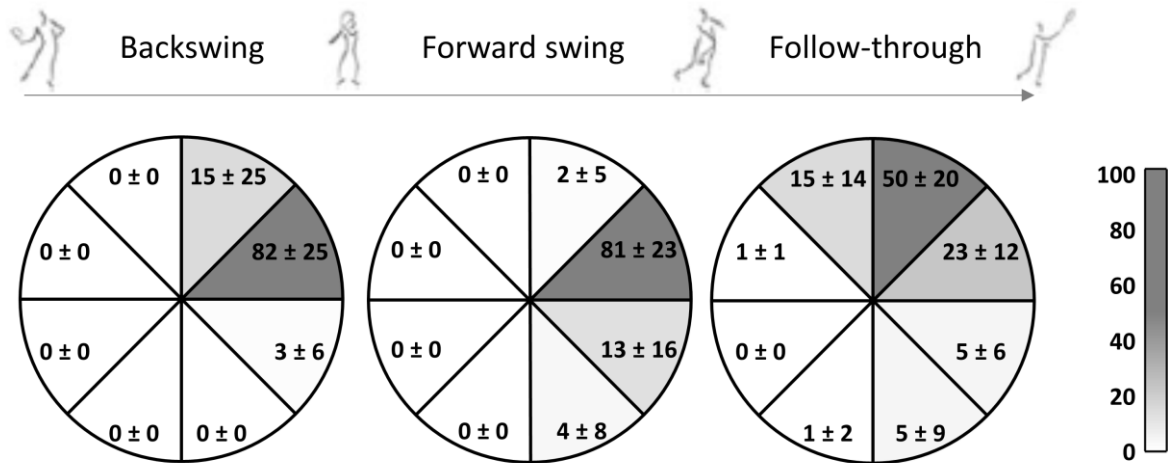


573

574

575

576 **Figure 5.** Mean \pm standard deviation distribution (%) of the glenohumeral contact forces
577 during the forehand drives with respect to the stroke phase. As no dependency between the
578 forehand drive technique and the glenoid section was observed, values for the flat and topspin
579 forehand drives were averaged.



580